


 Cite this: *Nanoscale*, 2024, **16**, 1415

Tumor-activated targetable photothermal chemotherapy using IR780/zoledronic acid-containing hybrid polymeric nanoassemblies with folate modification to treat aggressive breast cancer†

 Yu-Ling Liu,^a Tzu-Hao Wang,^a Nien-Tzu Yeh,^a Wei-Jen Huang,^a
 Bor-Show Tzang,^{b,c,d,e} I-Ting Wu,^b Hao-Yang Chin,^b Shang-Hsiu Hu,^f
 Tsai-Ching Hsu^{*b,d,e} and Wen-Hsuan Chiang^{†a}

To effectively treat aggressive breast cancer by tumor-activated targetable photothermal chemotherapy, in this work, folate (FA)-modified hybrid polymeric nanoassemblies (HPNs) with a poly(ethylene glycol) (PEG)-detachable capability are developed as vehicles for tumor-targeted co-delivery of IR780, a lipophilic photothermal reagent, and zoledronic acid (ZA), a hydrophilic chemotherapy drug. Through hydrophobic interaction-induced co-assembly, IR780 molecules and ZA/poly(ethylenimine) (PEI) complexes were co-encapsulated into a poly(lactic-co-glycolic acid) (PLGA)-rich core stabilized by the amphiphilic FA-modified D- α -tocopheryl poly(ethylene glycol) succinate (FA-TPGS) and acidity-sensitive PEG-benzoic imine-octadecane (C18) (PEG-b-C18) conjugates. The developed FA-ZA/IR780@HPNs with high ZA and IR780 payloads not only showed excellent colloidal stability in a serum-containing milieu, but also promoted IR780-based photostability and photothermal conversion efficiency. Furthermore, for FA-ZA/IR780@HPNs under simulated physiological conditions, the premature leakage of IR780 and ZA molecules was remarkably declined. In a mimetic acidic tumor microenvironment, the uptake of FA-ZA/IR780@HPNs by FA receptor-overexpressed 4T1 breast cancer cells was remarkably promoted by PEG detachment combined with FA receptor-mediated endocytosis, thus effectively hindering migration of cancer cells and augmenting the anticancer efficacy of photothermal chemotherapy. Notably, the *in vivo* studies demonstrated that the FA-ZA/IR780@HPNs largely deposited at 4T1 tumor sites and profoundly suppressed tumor growth and metastasis without severe systemic toxicity upon near infrared (NIR)-triggered IR780-mediated hyperthermia integrated with ZA chemotherapy. This work presents a practical strategy to treat aggressive breast tumors with tumor-triggered targetable photothermal chemotherapy using FA-ZA/IR780@HPNs.

 Received 7th November 2023,
 Accepted 11th December 2023
 DOI: 10.1039/d3nr05637f

rsc.li/nanoscale
^aDepartment of Chemical Engineering, National Chung Hsing University, Taichung 402, Taiwan. E-mail: whchiang@dragon.nchu.edu.tw
^bInstitute of Medicine, Chung Shan Medical University, Taichung 402, Taiwan. E-mail: hrc@csmu.edu.tw
^cDepartment of Biochemistry, School of Medicine, Chung Shan Medical University, Taichung 402, Taiwan

^dImmunology Research Center, Chung Shan Medical University, Taichung 402, Taiwan

^eClinical Laboratory, Chung Shan Medical University Hospital, Taichung 402, Taiwan

^fDepartment of Biomedical Engineering and Environmental Sciences, National Tsing Hua University, Hsinchu 300, Taiwan

 † Electronic supplementary information (ESI) available. See DOI: <https://doi.org/10.1039/d3nr05637f>

1. Introduction

The combination of photothermal therapy (PTT) and chemotherapy is one of the most common cancer treatments due to its better therapeutic efficacy than that of single therapies.^{1–4} Nevertheless, traditional photothermal chemotherapy has several drawbacks including a short blood circulation half-life, low intracellular delivery and poor tumor accumulation. To overcome these obstacles, taking advantage of the natural enhanced permeability and retention (EPR) effect of solid tumors, a variety of nanoparticles such as liposomes,^{5,6} polymeric assemblies,^{1,7–9} and metal organic frameworks^{2,10,11} have been developed as drug vehicles to achieve tumor-targeted delivery in photothermal chemotherapy. For example,

for effective cancer phototherapy, Park's group developed photothermally augmented therapeutic liposomes that encapsulate the photothermal agent indocyanine green (ICG) and the anticancer drug cisplatin to synergize chemotherapy and hyperthermia.⁵ Through the ICG-mediated photothermal effect, the release of cytotoxic cisplatin molecules from these liposomes was considerably promoted. The phototherapeutic studies demonstrated that the co-delivery of ICG and cisplatin by liposomes amplified therapeutic effects both *in vitro* in cancer cells and *in vivo* in mouse tumor models superior to single chemotherapy or photothermal therapy. Furthermore, as reported by Yang *et al.*,⁹ in order to accomplish near infrared (NIR)-activated cancer precision therapy in a remote-controlled manner, ICG-conjugated and bioactive compound gambogic acid (GA)-loaded polymeric micelles (GA@PEG-TK-ICG PMs) were produced *via* the self-assembly of the reactive oxygen species (ROS)-sensitive thioketal (TK)-linked amphiphilic polymer poly(ethylene glycol)-thioketal-ICG (PEG-TK-ICG). Under 808 nm laser irradiation, the GA@PEG-TK-ICG PMs realized ICG-mediated hyperthermia for PTT, and ROS as the feedback stimulate the micelles toward the tumor-specific liberation of GA, which could serve as not only a chemotherapy drug to directly kill tumor cells but also a heat shock protein 90 inhibitor to realize the photothermal sensitization. Note that most of the aforementioned nanoparticles exhibited PEG-rich hydrophilic surfaces, thereby decreasing their removal by the reticuloendothelial system (RES) and prolonging the blood circulation time to promote their tumor deposition upon the EPR effect.^{12–14} However, the hydrated PEG layer surrounding the surfaces of therapeutic nanoparticles has been demonstrated to impede their internalization by cancer cells, thus being unfavorable for intracellular drug delivery and anticancer potency.^{15–17}

To address the “PEG dilemma” issue, some tumor microenvironment-responsive PEG-detachable drug nanocarriers have been developed.^{15–23} More importantly, one unique tactic that is the “sequential-targeting” approach: PEGylation-aided “passive targeting” followed by dePEGylation/ligand exposure-induced “active targeting” has been verified to effectively promote the delivery efficiency of drug payloads to both the tumor sites and cancer cells.^{8,24–28} For example, Li's group adopted the strategy of “tumor-triggered targeting” to create dual-pH-responsive chitosan (CHI)/mesoporous silica nanoparticles (MSNs) coated with the targeting peptide adamantane-glycine-arginine-glycine-aspartic acid-serine (Ad-GRGDS) and methoxy poly(ethylene glycol) benzaldehyde (mPEG-CHO) for tumor-targeted delivery of doxorubicin (DOX).²⁴ Through dynamic protection of PEG, the obtained DOX-loaded nanoparticles were “stealthy” at pH 7.4, but upon dePEGylation driven by hydrolysis of benzoic imine bonds between CHI and mPEG, they efficiently exposed the shielded targeting peptide and the positive charges of CHI in the weakly acidic milieu (pH_c 6.5–7.0) to realize “tumor-triggered targeting”. Furthermore, as reported by Huang *et al.*,²⁵ in order to enhance the delivery of an anticancer drug, SN38, to cancer cells within tumor hypoxia, tumor microenvironment-

responsive nanoparticles were fabricated by the assembly of poly(lactic acid-co-glycolic acid)-grafted hyaluronic acid (HA-g-PLGA) together with SN38 in the aqueous phase, followed by covering the nanoparticle surface with a layer of mPEG-*b*-poly(histamine methacrylamide) (mPEG-*b*-PHMA) *via* hydrophobic association. The uptake of these SN38-carrying nanoparticles by CD44-overexpressed tumor cells, including cancer cells and tumor-associated macrophages (TAMs), was significantly increased by tumor acidity-triggered mPEG-*b*-PHMA detachment and HA exposure, thus promoting the delivery of the chemotherapeutic agent into hypoxic tumors by TAM-mediated hitchhiking transport. Despite the remarkable progress in the nanoparticle-based drug delivery systems engineered by tumor microenvironment-triggered dePEGylation and tumor targeting, to the best of our knowledge, most of these nanocarriers realized only single PTT or chemotherapy with limited efficacy.

Considering the pros and cons of the aforementioned studies, to largely boost the antitumor efficacy of photothermal chemotherapy, it is essential to create versatile drug nanocarriers capable of co-delivering chemotherapeutic drugs and photothermal agents to tumor sites and activating tumor-triggered specific targeting. To this end, folate (FA)-decorated hybrid polymeric nanoassemblies (HPNs) with a acidity-sensitive PEG-detachable ability were designed herein as vehicles for the co-delivery of IR780, a photothermal agent, and zoledronic acid (ZA), a third-generation bisphosphonate for the inhibition of osteolysis and breast cancer bone metastasis, to achieve tumor-activated targetable photothermal chemotherapy. To the best of our knowledge, very few studies on the tumor-targeted delivery in ZA/IR780-mediated photothermal chemotherapy have been reported due to a significant difference in the water solubility of IR780 and ZA that largely increases the difficulty of nano-formulation design. Firstly, amphiphilic FA-conjugated tocopherol polyethylene glycol succinate (FA-TPGS) and acidity-sensitive PEG-benzoic imine-octadecane (PEG-*b*-C18) used as the key materials for tumor-triggered targeting of HPNs were synthesized. Through ionic pairings of bisphosphonate-bearing ZA molecules and amine-rich poly(ethylenimine) (PEI) segments, the hydrophobicity of ZA molecules was promoted. Next, FA-modified ZA/IR780-loaded HPNs (FA-ZA/IR780@HPNs) were obtained by hydrophobic interaction-induced co-assembly of PLGA segments, IR780 molecules, ZA/PEI ionic complexes, FA-TPGS and PEG-*b*-C18 conjugates in a basic solution. The resulting FA-ZA/IR780@HPNs with high ZA and IR780 payloads not only exhibited low drug leakage, but also enhanced the photostability and photothermal conversion efficiency of IR780 molecules. Moreover, the *in vitro* cellular uptake and cytotoxicity studies revealed that the exposed FA moieties of FA-ZA/IR780@HPNs due to acidity-induced PEG detachment remarkably promoted their internalization by 4T1 breast cancer cells with FA receptor overexpression upon FA receptor-mediated endocytosis, thus not only hindering migration of cancer cells but also boosting the anticancer potency of the photothermal chemotherapy. Importantly, the NIR-triggered PTT of FA-ZA/IR780@HPNs selectively accumulated in tumor regions led to significant tumor ablation and remarkably

inhibited cancer metastasis by combining with ZA-mediated chemotherapy.

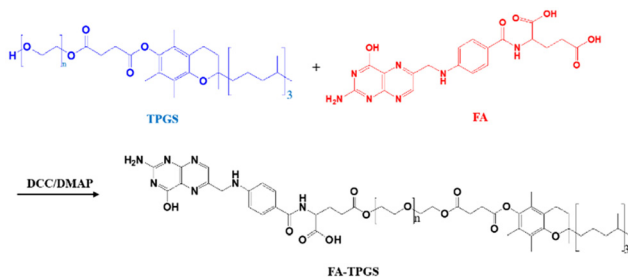
2. Experimental section

2.1. Materials

PEG-*b*-C18 conjugates utilized in this work were synthesized and characterized according to our previous report.²⁹ ZA was acquired from Tokyo Chemical Industry, Co., Ltd (Japan). PLGA (LA/GA 75/25, I.V. 0.18 dl g⁻¹, hydroxyl terminated) was purchased from Green Square (Taiwan). Branched PEI (M.W. = 1.8 kDa) was obtained from Alfa Aesar (USA). IR780 iodide dye, folate (FA, 97%), poly(ethylene glycol) methyl ether (mPEG-OH, average M_n 5000), propidium (PI, 94%), RPMI-1640 medium, and Hoechst 33342 (>98%) were purchased from Sigma-Aldrich (USA). TPGS (M.W. = 1513 g mol⁻¹) was obtained from Carbosynth Ltd (UK). Fetal bovine serum (FBS) was purchased from Hyclone (USA). 3-(4,5-Dimethylthiazol-2-yl)-2,5-diphenyltetrazolium bromide (MTT) was obtained from Alpha Biochemistry (Taiwan). Calcein-AM was obtained from AAT Bioquest (USA). Deionized water was produced using a Milli-Q Synthesis system (18 MΩ, Millipore). All other chemicals were reagent grade and used as received. 4T1 (murine breast cancer cell line) and TRAPM-C1 (murine prostate cancer cell line) were obtained from the Food Industry Research and Development Institute (Hsinchu City, Taiwan).

2.2. Synthesis and characterization of FA-TPGS adducts

The detailed synthetic pathway of FA-TPGS is presented in Scheme 2. TPGS (1 g, 0.65 mmol), FA in 5-fold molar excess with respect to TPGS, DCC (in 5-fold molar excess) and DMAP (equimolar) were dissolved in anhydrous DMSO (5.0 mL) and the reaction was carried out under stirring at 40 °C for 3 days. The solution was filtered to remove the byproduct dicyclohexylcarbodiurea (DCU), followed by dialysis (Cellu Sep MWCO 1000) against DMSO for 3 days to eliminate the residual DCU, unreacted FA and DMAP. After being dialyzed against deionized water for 1 day to remove DMSO, the purified solution was lyophilized to collect the final product. The structure of FA-TPGS adducts was characterized by proton nuclear magnetic resonance (¹H-NMR) spectroscopy (Agilent DD2 600 MHz NMR spectrometer) using DMSO-*d*₆ as the solvent.



Scheme 2 Synthetic routes and chemical structures of FA-TPGS conjugates.

2.3. Preparation of cargo-loaded HPNs

Various payload-carrying HPNs coated with either TPGS or FA-TPGS adducts were fabricated by the one-step nanoprecipitation method. For instance, the FA-decorated ZA/IR780-encapsulated HPNs (hereinafter referred to as FA-ZA/IR780@HPNs) were prepared as follows. First, ZA (2.0 mg) dissolved in pH 8.5 Tris buffer (0.85 mL) was added to 0.85 mL of pH 6.0 Tris buffer containing PEI (5.7 mg) and then stirred for 30 min to obtain the ZA/PEI ionic complexes. Then, PLGA (6.0 mg), FA-TPGS (0.8 mg), PEG-*b*-C18 (2.0 mg) and IR780 (0.6 mg) dissolved in DMSO (0.3 mL) were dropwise added to the ZA/PEI-containing aqueous solution (1.7 mL) under stirring. The mixed solution was gently stirred at 25 °C for 30 min. The obtained FA-ZA/IR780@HPN suspension was dialyzed (Cellu Sep MWCO 6000–8000) against pH 8.0 phosphate buffer (10 mM) at 4 °C to remove DMSO, unloaded ZA and IR780 molecules. For comparison, the IR780@HPNs with PEI addition, ZA@HPNs and ZA/IR780@HPNs were also fabricated in a similar manner.

2.4. Characterization of payload-carrying HPNs

The particle size, size distribution (polydispersity index, PDI) and zeta potential of various cargo-carrying HPNs dispersed in aqueous solutions were measured using a Litesizer 500 (Anton Paar, USA). The data shown herein represent an average of at least three measurements. The morphology of FA-ZA/IR780@HPNs negatively stained with 2 wt% phosphotungstic acid hydrate was observed using a transmission electron microscope (TEM) (JEOL JEM-1400 CXII microscope). The absorption spectra of free IR780 molecules and IR780-carrying HPNs in phosphate buffered saline (PBS) were obtained using a UV/Vis spectrophotometer (V730, JASCO, Japan). Various IR780-carrying HPNs and free IR780 molecules dispersed in 1.0 mL PBS (IR780 concentration = 80 μM) were irradiated with a NIR laser of 808 nm (1.0 W cm⁻²) for 5 min and then cooled down to room temperature (in 5 min) by turning off the light source. The solution temperatures were recorded with an infrared thermal imaging camera (Thermo Shot F20, NEC Avio Infrared Technologies, Germany). Based on the data from the heating/cooling status, the photothermal conversion efficiency of various IR780-carrying HPNs and free IR780 molecules was calculated using the formula reported in the literature.^{30,31}

The ZA loading efficiency and content of different ZA-carrying HPNs were determined by the previously established method as described in the ESI.† Furthermore, to quantify IR780 encapsulated within HPNs, the absorbance of the IR780-containing HPN solution after 100-fold dilution with phosphate buffer (pH 7.4, 0.01 M) at 785 nm was determined using a UV/Vis spectrophotometer. The IR780 calibration curve used for drug loading characterization is presented in Fig. S1.† The IR780 loading efficiency (DLE) and loading content (DLC) were calculated using the following formulas:

$$\text{DLE (\%)} = \left(\frac{\text{weight of IR780 loaded}}{\text{weight of IR780 in feed}} \right) \times 100\%$$

$$\text{DLC}(\%) = \left(\frac{\text{weight of IR780 loaded}}{\text{total weight of IR780 - carrying HPNs}} \right) \times 100\%$$

To evaluate the aqueous photostability of IR780, the characteristic IR780 absorbance of free IR780 and various IR780-carrying HPNs (IR780 concentration = 8 μM) in PBS (pH 7.4, 0.15 M) exposed to a daylight lamp at 37 $^{\circ}\text{C}$ was determined over time using a UV/Vis spectrophotometer. The IR780 absorbance (Abs) measured at different time intervals was normalized with the following formula.

$$\text{Normalized absorbance}(\%) = \frac{\text{Abs}_{\text{at different time intervals}}}{\text{Abs}_{\text{at the beginning}}} \times 100\%$$

2.5. *In vitro* cargo release study characterization of payload-carrying HPNs

For ZA liberation measurement, the ZA-carrying HPN dispersion (1.0 mL) was dialyzed (Cellu Sep MWCO 6000–8000) against PBS of pH 7.4 and 5.5 (ionic strength 0.15 M, 15 mL), respectively, at 37 $^{\circ}\text{C}$. At the prescribed time intervals, 1.0 mL of dialysate (pH 5.5 or 7.4) was taken for analysis and replaced with an equivalent volume of fresh buffer. The ZA concentration was measured by HPLC as described in the ESI.†

For the IR780 release study, the IR780-containing HPN solution (1.0 mL) was dialyzed (Cellu Sep MWCO 6000–8000) against PBS of pH 7.4 and 5.5 (ionic strength 0.15 M, 20 mL), respectively, at 37 $^{\circ}\text{C}$. The internal sample was withdrawn periodically and the absorbance at 780 nm was measured. The sample solution was placed back into the dialysis tube after each analysis. The cumulative IR780 release (%) was calculated using the following equation:

$$\text{Cumulative IR780 release}(\%) = \left(\frac{\text{Initial IR780 absorbance} - \text{IR780 absorbance at the predetermined time points}}{\text{initial IR780 absorbance}} \right) \times 100\%$$

2.6. *In vitro* cellular uptake

4T1 cells (1.5×10^5 cells per well) seeded onto 22 mm round glass coverslips in 6-well plates were incubated with free IR780 molecules, FA-ZA/IR780@HPNs and ZA/IR780@HPNs (IR780 concentration = 5 μM) at pH 7.4 and 6.5, respectively, for 1 h. After being washed three times with HBSS and immobilized with 4% formaldehyde, the cell nuclei were stained with Hoechst 33342. The cellular images were observed using a laser scanning confocal microscope (LSCM) (Olympus, Fluo View FV3000, Japan) equipped with a Hoechst set (Ex. 405 nm) and an IR780 set (Ex. 640 nm). On the other hand, the internalization of free IR780 molecules, FA-ZA/IR780@HPNs and ZA/IR780@HPNs (IR780 concentration = 1.5 μM) by 4T1 cells at 37 $^{\circ}\text{C}$ and at pH 7.4 and 6.5, respectively, was assessed using a FACSCalibur flow cytometer (BD Bioscience). After 1 h incubation and detachment with trypsin-EDTA solution, the treated 4T1 cells (2×10^5 cells per well) were dispersed in PBS (1.0 mL). The fluorescence intensity of a minimum of 1×10^4 cells was analyzed and is displayed on a log scale.

2.7. Inhibition of *in vitro* 4T1 cell migration

4T1 cells (1.5×10^5 cells per well) formed a confluent monolayer, followed by scratching to generate a gap. Subsequently, cells were incubated with free ZA molecules, free ZA/IR780 mixtures and various payload-carrying HPNs at a concentration equal to 1.65 μM of ZA and 0.19 μM of IR780 at pH 7.4 and 6.5, respectively, for 24 h. Images of the scratches were obtained at 0 and 24 h with a NIB-100F inverted fluorescence biological microscope (Nanjing Jiangnan Novel Optics Co., Ltd, China) and ImageJ software was utilized to quantify migration. The cell migration rate (R_M) was calculated using the following equation:

$$R_M = \frac{(\text{width of initial gap} - \text{width of final gap})}{\text{cell migration time}}$$

2.8. *In vitro* anticancer effect of photothermal chemotherapy

To evaluate the anticancer efficacy of single chemotherapy, 4T1 cells (1×10^4 cells per well) were seeded in a 96-well plate and incubated in RPMI-1640 containing 10% FBS and 1% penicillin at 37 $^{\circ}\text{C}$ for 24 h. The spent medium was then replaced with 100 μL of fresh RPMI-1640 (pH 7.4 or 6.5) containing free ZA molecules, free IR780 molecules, free ZA/IR780 mixtures or various cargo-loaded HPNs and was further incubated for additional 24 h. Afterward, 100 μL of MTT (0.25 mg mL⁻¹) was added into each well, followed by incubation at 37 $^{\circ}\text{C}$ for 3 h. After removing the culture medium, 100 μL of DMSO was added into each well to dissolve the precipitate, followed by the determination of the absorbance at 570 nm using a microplate reader (BioTek 800 TS).

To further explore the anticancer potency of photothermal chemotherapy, 4T1 cells (1×10^5 cells per well) seeded in a 12-well plate were incubated with 1.0 mL of RPMI-1640 (pH 7.4 or 6.5) containing free ZA molecules, free IR780 molecules, a free ZA/IR780 mixture or various cargo-loaded HPNs (ZA concentration = 6.25 μM , IR780 concentration = 0.75 μM) at 37 $^{\circ}\text{C}$ for 24 h. After being washed twice with PBS, cells were detached with trypsin-EDTA and centrifuged (1500 rpm). The obtained cell pellets were irradiated with a NIR 808 nm laser (1.25 W cm⁻²) for 5 min and then reseeded in a 12-well plate for additional 12 h incubation. MTT (0.25 mg mL⁻¹, 1.0 mL) was then added into each well, followed by incubation at 37 $^{\circ}\text{C}$ for 3 h. After discarding the culture medium, DMSO (1.0 mL) was added to dissolve the precipitate and the absorbance of the resulting solution at 570 nm was determined using a BioTek 800TS microplate reader.

On the other hand, the anticancer effect of photothermal chemotherapy delivered by FA-ZA/IR780@HPNs on 4T1 cells was assessed by fluorescence staining of live/dead cells. 4T1 cells (1.5×10^5 cells per well) seeded in a 12-well plate were incubated with FA-ZA/IR780@HPNs (ZA concentration = 3.13 μM , IR780 concentration = 0.38 μM) at pH 7.4 and 6.5, respectively, for 24 h. Subsequently, cells were irradiated with an 808 nm NIR laser (1.25 W cm⁻²) for 5 min and gently washed twice with PBS to avoid washing off dead cells. A calcein AM (0.2 μM) and propidium iodide (PI, 25 $\mu\text{g mL}^{-1}$)

mixture solution (500 μL) was added and kept at room temperature for 30 min. The cellular images were acquired using a NIB-100F inverted fluorescence biological microscope.

2.9. Animals and tumor model

Female BALB/c mice (5–6 weeks old) purchased from the National Laboratory Animal Center (Taiwan) were cared according to the Guidance Suggestions for the Care and Use of Laboratory Animals, approved by the Administrative Committee on Animal Research in the Chung Shan Medical University (Taiwan) (IACUC Approval No: 2528). To establish a tumor model, 2×10^6 4T1 cells were subcutaneously injected into the right thigh of mice. 10 days post-inoculation, the tumor model was established. Tumor volume (V) was calculated as follows: $V = L \times W^2/2$, where W is the tumor measurement at the widest point and L is the tumor dimension at the longest point.

2.10. *In vivo* imaging and biodistribution

When the tumor volume reached 90–110 mm^3 , mice were randomly divided into 4 groups and intravenously injected with PBS, free ZA/IR780 mixtures, ZA/IR780@HPNs and FA-ZA/IR780@HPNs, respectively, at an IR780 dosage of 1.0 mg kg^{-1} . The fluorescence signals of IR780 (Ex. 710 nm and Em. 760 nm) at 2, 4, 6, 24 and 48 h post-injection were collected with an IVIS imaging system (IVIS Lumina II, Caliper, LifeSciences, MA, USA). The treated mice were sacrificed by CO_2 euthanasia at 48 h post-injection and the major organs and tumor were gathered for imaging by IVIS.

2.11. *In vivo* temperature measurements upon NIR irradiation

The procedure for the *in vivo* distribution investigation was followed. At 24 h post-injection, the tumor site of mice was irradiated with an 808 nm laser (1.25 W cm^{-2}) for 3 min. The infrared thermographic maps of mice and the tumor local temperature under NIR laser irradiation were obtained with an infrared thermal imaging camera (Thermo Shot F20, NEC Avio Infrared Technologies, Germany).

2.12. *In vivo* tumor growth inhibition

When the tumor volume of mice reached 90–110 mm^3 , mice were randomly divided into 7 groups ($n = 4$ per group): (i) PBS, (ii) free ZA/IR780 mixtures, (iii) ZA/IR780@HPNs, (iv) FA-ZA/IR780@HPNs, (v) free ZA/IR780 mixtures + NIR laser, (vi) ZA/IR780@HPNs + NIR laser and (vii) FA-ZA/IR780@HPNs + NIR laser. Mice in different groups were intravenously injected with the corresponding reagents at a ZA dosage of 3.2 mg kg^{-1} and an IR780 dosage of 1.0 mg kg^{-1} . Each group was treated with a total of two doses at days 0 and 5. At 24 h post-injection, the tumor site of mice in the prescribed groups was irradiated with an 808 nm laser (1.25 W cm^{-2}) for 5 min. The tumor volume and body weight of different groups were measured every two days until 20 days post-treatment. To evaluate the antitumor efficacy, the relative tumor volumes (V/V_0) of different groups were obtained by the normalization of the

tumor volumes (V) against the original tumor volume (V_0). After all mice were euthanized, the tumors and main organs including the heart, liver, spleen, lungs, and kidneys were gathered. Then, the tumor and spleen were weighed. The therapeutic index (TI) of different treatments was calculated using the following formula: $\text{TI} (\%) = (1 - (\text{weight of tumor in the experimental group})/(\text{weight of tumor in the control group}))$.

The harvested tumors and organs were fixed with 4% paraformaldehyde and then processed routinely in paraffin. Afterward, the tumors and organs were sectioned into 4 μm thick slices and stained with hematoxylin and eosin (H&E) and Ki67, respectively, followed by examination using an Olympus IX70 inverted microscope (Japan).

2.13. Statistical analysis

Data are reported as mean \pm SD. The differences among groups were determined using one-way or two-way ANOVA analysis; ns > 0.05, * p < 0.05, ** p < 0.01, *** p < 0.001.

3. Results and discussion

3.1. Synthesis and characterization of FA-TPGS

The FA-TPGS adducts were synthesized by DCC/NHS-mediated esterification of FA with TPGS. As revealed in Fig. 1, in addition to the appearance of characteristic proton signals of TPGS segments, the proton signals of FA moieties were observed in the $^1\text{H-NMR}$ spectrum of FA-TPGS, being indicative of the successful modification of TPGS with FA. In view of the signal integral ratio of the benzene ring (δ 7.61 ppm) of FA and the methyl group (δ 0.81 ppm) of TPGS, the conjugation efficiency was attained to be ca. 88%.

3.2. Preparation and characterization of payload-carrying HPNs

In our previous work,³² it was found that the ionic pairings of positively-charged PEI segments with negatively-charged ZA molecules largely increased the encapsulation of ZA into the PLGA-rich core of hybrid nanoparticles. Therefore, in this study, the PEI segments were employed in the preparation of HPNs. Various cargo-carrying HPNs (with or without FA decoration) were attained by one-step co-assembly of PLGA,

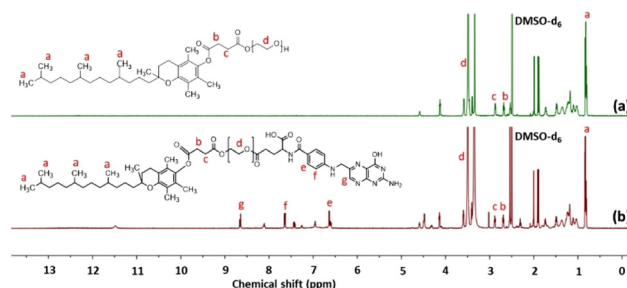


Fig. 1 $^1\text{H-NMR}$ spectra of (a) TPGS and (b) FA-TPGS in DMSO-d_6 .

FA-TPGS or TPGS, PEG-*b*-C18, ZA/PEI complexes and/or IR780 in basic aqueous solution. Through the hydrophobic anchoring of a long alkyl chain from vitamin E moieties of TPGS and octadecane of PEG-*b*-C18 on the surfaces of HPNs, the resulting payload-containing HPNs were well suspended in aqueous solutions by PEG-rich hydrophilic surfaces (Fig. 2a). Notably, the hydrophobic IR780 molecules incorporated into HPNs showed an appreciable red shift in the feature absorption peak from 775 to 785 nm (Fig. 2a), indicating the extensive associ-

ation of IR780 with the lipophilic alkyl chains of PEG-*b*-C18 and TPGS anchored on the PLGA cores. Similar results have also been found elsewhere.^{33,34} As presented in drug loading data (Table 1), for various payload-carrying HNP, the loading efficiency of ZA and/or IR780 molecules was determined to be over 77%, signifying that IR780 and ZA molecules could be sufficiently encapsulated within the PLGA-rich core of HPNs. As shown in Table 1, the particle size of payload-carrying HPNs was somewhat larger than that of drug-free HPNs, indicating that the encapsulation of IR780 or ZA/PEI complexes within PLGA cores could enlarge the particle size. Various cargo-carrying HNP dispersed in pH 7.4 PBS showed similar nano-scaled particle sizes and monomodal size distributions (Fig. 2b and Table 1), illustrating that the loading of single or dual drugs, and surface coating of TPGS or FA-TPGS do not remarkably affect the colloidal size of payload-containing HNP. Furthermore, the FA-ZA/IR780@HPNs exhibited a well-dispersed and spherical shape as observed in their TEM images (Fig. 2c).

Notably, with the solution pH being reduced from 7.4 to 5.0, the zeta potentials of payload-carrying HPNs changed from virtually neutral to appreciably positive values (Fig. 2d). Obviously, the acidity-triggered hydrolysis of the benzoic imine bond in PEG-*b*-C18 adducts led to the PEG detachment from the surfaces of HPNs, thus exposing positive charges of protonated PEI segments.²⁹ By contrast, under the same pH stimulation, only a slight change in the zeta potential of PEG non-detachable ZA/IR780@HPNs was observed (Fig. S2†). This is because the PEG-stearic acid (PEG-C18) lacking acid-labile bond anchored on the surfaces of ZA/IR780@HPNs largely shielded the positively-charged PEI segments in the absence of dePEGylation. Furthermore, the ¹H-NMR spectrum of PEG-*b*-C18 conjugates receiving acid treatment (pH 6.5 for 3 h) showed the appearance of the proton signal of the aldehyde group at δ 10.1 ppm and the disappearance of the proton signal of the imine group at δ 8.5 ppm (Fig. S3†), strongly suggesting the acidity-induced hydrolysis of the benzoic imine bond of mPEG-*b*-C18. Based on the above findings, such a dePEGylation of payload-carrying HPNs with FA decoration was assumed to activate FA-mediated tumor targeting. Additionally, the mean particle sizes of the cargo-loaded HPNs with or without FA modification were virtually unchanged in the milieu pH 5.0–7.4 as revealed in Fig. S4.† It is worth mentioning that the FA-ZA/IR780@HPNs not only exhibited the dePEGylation performance but also retained the well-dispersed colloidal structure under weak acidic conditions, an important prerequisite for maximizing the exposure of FA moieties on the HPN surfaces to enhance the tumor targeting efficiency (Scheme 1).

To assess the aqueous photostability of IR780 encapsulated within HPNs, the change in the absorbance of various IR780-carrying HPNs in pH 7.4 PBS at 37 °C exposed to white light over time was recorded by UV/Vis spectroscopy (Fig. S5†). Note that the normalized absorbance of free IR780 molecules significantly declined over 4 h, while only a minor decrease in absorbance was obtained for various IR780-containing HPNs

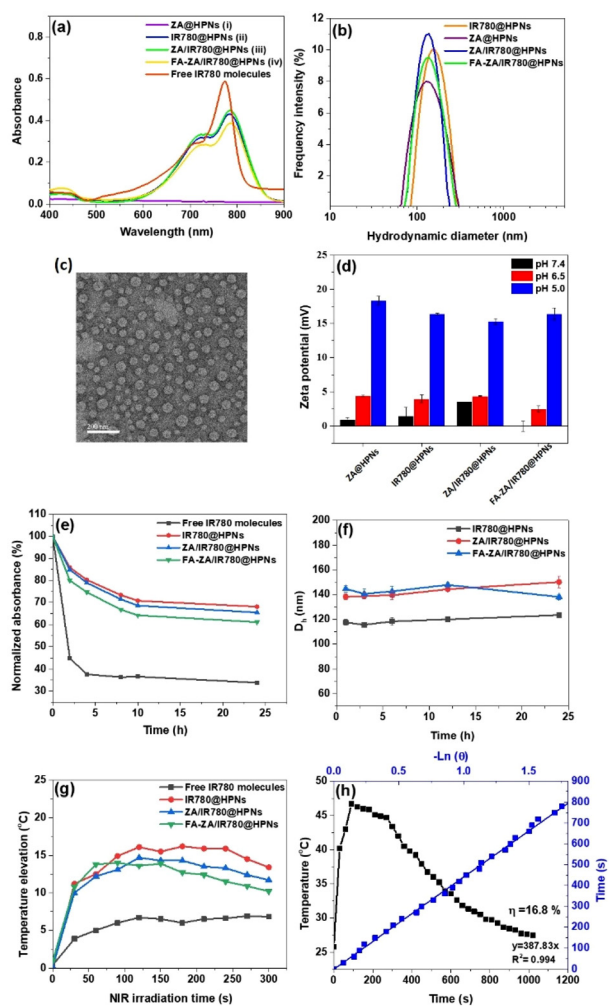
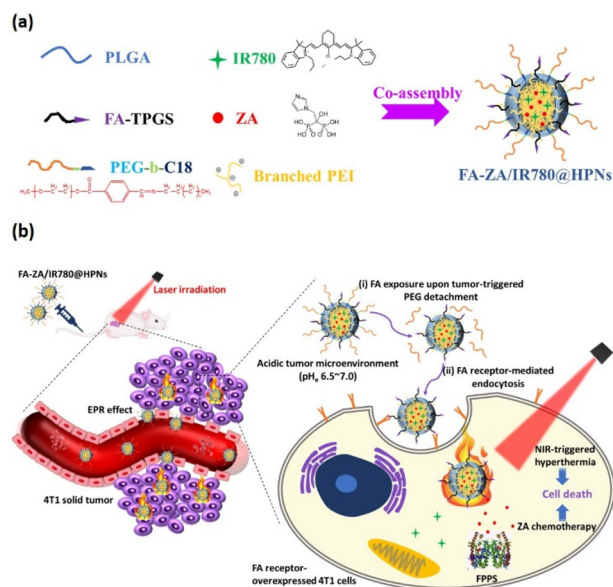


Fig. 2 (a) UV/Vis spectra and photographs of aqueous solutions of (i) ZA@HPNs, (ii) IR780@HPNs, (iii) ZA/IR780@HPNs, and (iv) FA-ZA/IR780@HPNs. (b) DLS particle size distribution profiles of various cargo-loaded HPNs in pH 7.4 PBS. (c) TEM image of FA-ZA/IR780@HPNs. Scale bar is 200 nm. (d) Zeta potential of cargo-loaded HPNs in aqueous solutions of different pH ($n = 3$). (e) Normalized absorbance of free IR780 molecules and various IR780-loaded HPNs in pH 7.4 PBS at different time intervals. (f) Colloidal stability of various cargo-loaded HPNs in 10% FBS-containing PBS at 37 °C ($n = 3$). (g) Temperature change of free IR780 molecules and different IR780-containing HPNs in PBS during 808 nm NIR laser irradiation. (h) Temperature profile of FA-ZA/IR780@HPN solution (IR780 concentration = 80 μ M) after exposure to 808 nm laser irradiation (1.0 W cm^{-2}) for a single on/off cycle, and plot of cooling time versus negative logarithm of the temperature driving force.

Table 1 DLS data and drug loading characteristics of drug-free HPNs and cargo-carrying HPNs ($n = 3$)

Sample	D_h (nm)	PDI	ZA LE (%)	ZA LC (wt%)	IR780 LE (%)	IR780 LC (wt%)
HPNs	128.9 ± 1.3	0.218 ± 0.037	—	—	—	—
IR780@HPNs	148.3 ± 5.5	0.223 ± 0.019	—	—	77.2 ± 1.1	3.19 ± 0.05
ZA@HPNs	140.7 ± 4.3	0.204 ± 0.033	83.0 ± 4.1	11.4 ± 0.57	—	—
ZA/IR780@HPN	156.7 ± 4.9	0.237 ± 0.013	85.7 ± 7.0	11.8 ± 0.97	88.7 ± 3.2	3.67 ± 0.13
FA-ZA/IR780@HPNs	151.9 ± 3.4	0.217 ± 0.038	81.7 ± 7.0	11.2 ± 0.97	85.5 ± 1.3	3.53 ± 0.05

**Scheme 1** Schematic illustration of (a) colloidal structure of FA-ZA/IR780@HPNs and (b) antitumor effect of tumor-triggered targetable photothermal chemotherapy delivered by FA-ZA/IR780@HPNs.

(Fig. 2e). For IR780-carrying HPNs, such an enhanced photostability was primarily attributed to the protective effect of the PLGA-based core utilized as an IR780 reservoir that prevented IR780 from photobleaching and massive self-aggregation in the aqueous phase.^{33,35} Importantly, these cargo-carrying HPNs retained nearly unchanged particle size in 10% FBS-containing PBS over 24 h (Fig. 2f). Also, after being largely diluted with pH 7.4 PBS, these payload-containing HPNs still maintained virtually unvaried particle size (Fig. S6†). Notably, for ZA/IR780@HPNs without TPGS decoration, these nanoparticles tended to aggregate in FBS-containing PBS with time as reflected by their enlarged particle size (Fig. S7†). On the other hand, it was found that the IR780@HPNs lacking PEI segments were apt for aggregation into visible precipitates in pH 7.4 PBS, while the PEI-incorporated IR780@HPNs exhibited stable colloidal dispersion (Fig. S8†). Furthermore, these PEI-containing cargo-loaded HPNs stored in pH 7.4 PBS virtually maintained their particle size over 24 days (Fig. S9†). Obviously, the addition of PEI segments into HPNs not only formed ionic complexes with ZA molecules but also served as the stabilizer to enhance the colloidal stability of cargo-loaded HPNs. Based on these results, it was expected that the robust PLGA-rich core and the PEG/PEI/TPGS-covered surfaces of

cargo-carrying HPNs could effectively enhance their colloidal stability, thereby probably reducing the burst leakage of payloads and interparticle aggregation during blood circulation.

Next, the temperature of aqueous solutions of IR780-containing HPNs under irradiation of an 808 nm NIR laser was monitored using an infrared thermal imaging camera to evaluate their photothermal conversion capability. As revealed in Fig. 2g, at an IR780 concentration of 40 μM , during NIR laser irradiation (1.0 W cm^{-2}), the temperature elevation of the aqueous solutions of IR780-containing HPNs was appreciably higher than that of free IR780 suspension. Such a difference in the NIR-elicited photothermal effects between IR780-carrying nanoassemblies and free IR780 molecules was also observed elsewhere.^{33,36} Moreover, based on the photothermal heating-cooling curve of FA-ZA/IR780@HPNs (Fig. 2h), their photothermal conversion efficiency was determined to be *ca.* 16.8%, comparable to those of ZA/IR780@HPNs and IR780@HPNs (Fig. S10a and b†). In comparison with the above IR780-carrying HPNs, free IR780 molecules had a lower photothermal conversion efficiency of *ca.* 11.2% (Fig. S10c†). In view of these findings, it can be concluded that the encapsulation of IR780 molecules within HPNs could not only reduce their photobleaching impact during NIR irradiation but also avoid their aggregation, thus promoting their photothermal conversion effect. Furthermore, as expected, under NIR irradiation, the solution temperature was further elevated by increasing the concentration of IR780-carrying HPNs (Fig. S11†).

3.3. *In vitro* ZA and IR780 liberation from cargo-loaded HPNs

In this work, the *in vitro* drug release behavior of cargo-carrying HPNs was investigated by the dialysis method. As presented in Fig. 3a and b, compared to the quick outflow of free IR780 molecules across the dialysis tube in PBS of pH 7.4 and 5.5 (>60% over 4 h), IR780 liberated from IR780-containing HPNs under the same conditions was remarkably hindered (below 20% during 24 h). This clearly illustrates that the hydrophobic PLGA-rich core of cargo-loaded HPNs could potently retard the leakage of IR780 molecules from the colloidal structure. Moreover, the relatively low cumulative ZA release of ZA-carrying HPNs regardless of environment pH suggests that the encapsulation of ZA/PEI complexes into the hydrophobic PLGA-rich core could appreciably decline ZA burst release from HPNs (Fig. 3c and d). Despite the slow drug release profile of the ZA-carrying HPNs under weak acidic conditions (pH 5.5), this would not affect the potential clinical applications of these nanoparticles, as several previous studies

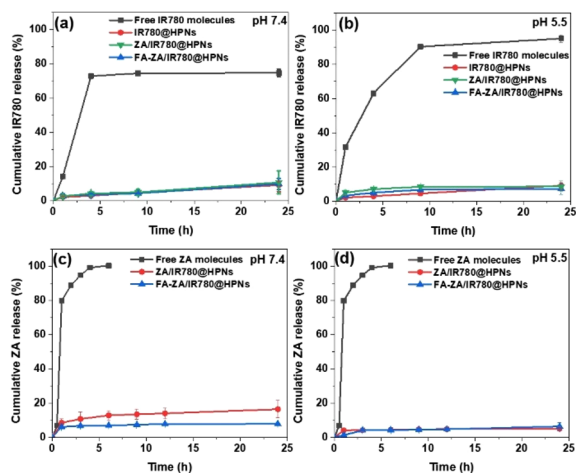


Fig. 3 Cumulative IR780 release profiles of various cargo-loaded HPNs in PBS of (a) pH 7.4 and (b) pH 5.5 at 37 °C ($n = 3$). Cumulative ZA release profiles of ZA/IR780@HPNs and FA-ZA/IR780@HPNs in PBS of (c) pH 7.4 and (d) pH 5.5 at 37 °C ($n = 3$). For comparison, diffusion of free IR780 and ZA molecules through the dialysis tube in pH 7.4 and 5.5 aqueous solutions is included.

pointed out that the gradual degradation of PLGA-rich nanoparticles in intracellular acidic endosomes/lysosomes upon the acid/enzyme-mediated PLGA hydrolysis led to drug release, thus killing cancer cells.^{37–39} Based on the above results, the payload-carrying HPNs are expected to be capable of preventing the premature leakage of ZA and IR780 molecules during blood circulation, thus maximizing the tumor-targeted delivery of photothermal chemotherapy.

3.4. *In vitro* tumor acidity-mediated cellular internalization

The effect of acidity-triggered PEG detachment and FA-mediated targeting of FA-ZA/IR780@HPNs on their cellular internalization was assessed using 4T1 cells with FA receptor overexpression as a cell model. As revealed in the LSCM images (Fig. 4a), with 1 h incubation at pH 7.4, IR780 delivered by ZA/IR780@HPNs was observed in a moderate amount in the cytoplasm of 4T1 cells, whereas quite a few free IR780 molecules were found intracellularly. Also, the quantified IR780 fluorescence intensity of 4T1 cells incubated with ZA/IR780@HPNs was appreciably 2-fold higher than that of cells treated with free IR780 molecules (Fig. 4b). Such a poor cellular uptake of free IR780 molecules relative to that of ZA/IR780@HPNs at pH 7.4 was attributed to that the massive intermolecular aggregation of lipophilic IR780 molecules in the culture medium largely retarded their cellular uptake. Similar observation on the low cellular uptake of free IR780 molecules was also reported elsewhere.^{40,41} Notably, when the culture pH was changed from 7.4 to 6.5, the intracellular IR780 fluorescence signals of 4T1 cells treated with ZA/IR780@HPNs markedly enhanced (Fig. 4a and b), consistent with the observation by flow cytometry (Fig. S12[†]). These results clearly indicate that the cellular uptake of ZA/IR780@HPNs by 4T1 cells in a weakly acidic milieu could be

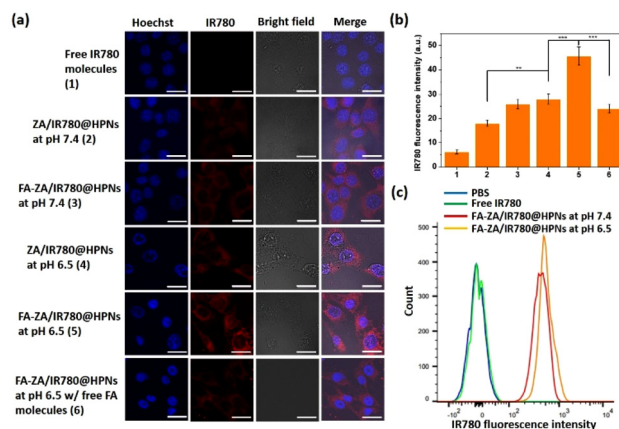


Fig. 4 (a) LSCM images and (b) quantified IR780 fluorescence signals of 4T1 cells incubated with either ZA/IR780@HPNs at pH 7.4 and 6.5 or FA-ZA/IR780@HPNs at pH 7.4 and 6.5 for 1 h (IR780 concentration = 5 μ M) ($n = 3$). Scale bars are 20 μ m. (c) Flow cytometric histograms of 4T1 cells incubated with FA-ZA/IR780@HPNs at pH 7.4 and 6.5 for 1 h (IR780 concentration = 1.5 μ M).

promoted upon the amplified affinity of HPNs with cancer cells due to acidity-induced PEG detachment. For FA-ZA/IR780@HPNs, the pH-dependent increase in cellular uptake was also confirmed by LSCM images and flow cytometric histograms (Fig. 4). More importantly, after being incubated with 4T1 cells at pH 6.5 for 1 h, the FA-ZA/IR780@HPNs exhibited remarkably boosted intracellular IR780 fluorescence signals by 1.6-fold in comparison with ZA/IR780@HPNs (Fig. 4a and b). Furthermore, the intracellular IR780 fluorescence of 4T1 cells incubated with FA-ZA/IR780@HPNs at pH 6.5 in the presence of free FA (2 μ M) appreciably decreased, indicating that the internalization of cargo-loaded HPNs by 4T1 cells was hindered since free FA molecules competed with HPNs for the FA receptors of 4T1 cells. Evidently, the FA exposure of FA-ZA/IR780@HPNs under mimic tumor acidity conditions owing to their PEG detachment prominently enhanced their uptake by 4T1 cells *via* FA receptor-mediated endocytosis (Scheme 1). As a result, it is expected that the effective intracellular co-delivery of ZA and IR780 payloads could boost the anticancer potency of photothermal chemotherapy.

3.5. Inhibition of 4T1 cell migration

Cancer-associated death is primarily caused by cancer metastasis. During tumor development, the deregulation of cell proliferation and movement facilitates the escape of cancer cells from the primary site to invade adjacent tissues, thus resulting in cancer metastasis.^{42,43} In order to prevent metastasis, it is essential to impede cancer cell migration and adhesion. Considering that ZA can diminish cell migration and proliferation by inhibiting farnesyl diphosphate synthase,^{43–46} we explored the capability of various ZA-carrying HPNs to inhibit 4T1 cell migration by the scratch wound healing assay. In this assay, this wound gap in a cell monolayer was created by

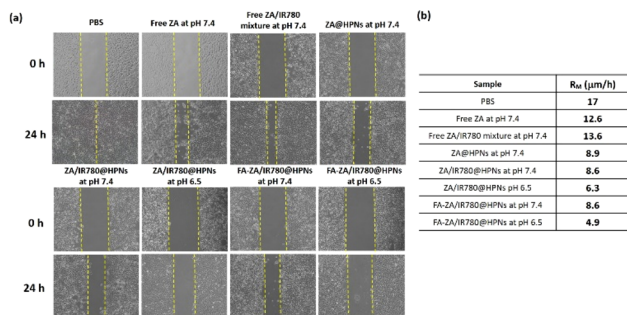


Fig. 5 (a) Representative images (magnification, $\times 40$) of the wound healing assay using 4T1 cells receiving various treatments. (b) Migration rate of 4T1 cells treated with various formulations.

scratching and “healing” was observed due to cell migration. As presented in Fig. 5a, PBS as control was unable to suppress 4T1 migration, while free ZA molecules and ZA/IR780 mixtures only slightly retarded the 4T1 cell motility. By contrast, various ZA-carrying HPNs incubated with 4T1 cells at pH 7.4 showed remarkably enhanced ability of inhibiting 4T1 cell migration. This indicates that these ZA-containing HPNs could promote intracellular ZA delivery compared to free ZA molecules with highly hydrophilic properties, thus moderately hindering the migration of 4T1 cells. With the culture pH being adjusted from pH 7.4 to 6.5, the invasion of 4T1 cells treated with ZA-containing HPNs was further inhibited, in particular for FA-ZA/IR780@HPNs. To quantify the anti-migration effect, the R_M of 4T1 cells receiving different treatments was obtained. As shown in Fig. 5b, the R_M (4.9) of 4T1 cells incubated with FA-ZA/IR780@HPNs at pH 6.5 is significantly lower than that (8.6) of cells treated with their counterparts at pH 7.4, that (6.3) of cells treated with ZA/IR780@HPNs at pH 6.5 and that (12.6) of cells incubated with free ZA molecules. The findings strongly suggest that the FA-ZA/IR780@HPNs in a weakly acidic environment displayed the best anti-migration potency *via* the boosted intracellular ZA delivery driven by acidity-activated PEG detachment and FA targeting.

3.6. *In vitro* photothermal chemotherapy

To investigate the anticancer efficacy of IR780-mediated NIR-elicited hyperthermia integrated with ZA chemotherapy, the viability of 4T1 cells treated with FA-decorated HPNs realizing single- and dual-modality therapies was evaluated by the MTT assay. As an essential control, 4T1 cells exposed to drug-free FA-HPNs ($4.7\text{--}75\ \mu\text{g mL}^{-1}$) at pH 7.4 or 6.5 for 24 h retained high viability around 80%, signifying the negligible cytotoxicity of these nanovehicles on cancer cells (Fig. 6a). As presented in Fig. S13a and b,† in the absence of NIR laser irradiation, the high viability (beyond 80%) of 4T1 cells treated with either free ZA ($6.25\text{--}50\ \mu\text{M}$) or IR780 molecules ($1.25\text{--}10\ \mu\text{M}$) was attained. Such low cytotoxicity of free hydrophilic ZA and hydrophobic IR780 molecules on 4T1 cells could be ascribed to their poor cellular uptake. Unexpectedly, the viability of 4T1 cells incubated with ZA/IR780 mixtures at pH 7.4 or 6.5 was appreciably

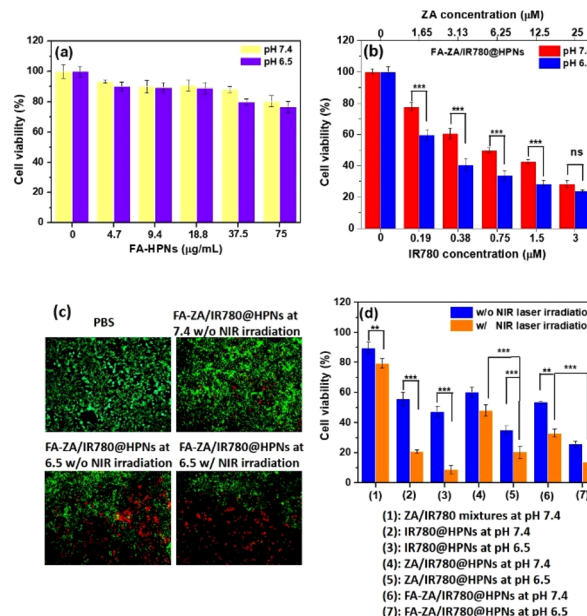


Fig. 6 Cell viability of 4T1 cells incubated with (a) FA-HPNs and (b) FA-ZA/IR780@HPNs at pH 7.4 and 6.5, respectively, for 24 h ($n = 3$). (c) Fluorescence images of 4T1 cells treated with FA-ZA/IR780@HPNs at pH 7.4 for 24 h without NIR laser irradiation or at pH 6.5 for 24 h with and without 5 min NIR laser irradiation. The viable cells were stained green with calcein AM, and the dead cells were stained red with PI. (d) Cell viability of 4T1 cells receiving different treatments (ZA concentration = $6.25\ \mu\text{M}$ and IR780 concentration = $0.75\ \mu\text{M}$, $n = 3$).

reduced by the increased drug concentration (Fig. S13c†). This may be ascribed to that the cellular uptake of the ZA/IR780 mixture could be promoted, thus increasing the intracellular ZA concentration to boost cytotoxicity, although the self-assembly of these mixed molecules at the molecular level is currently not clear. Note that, without NIR laser irradiation, the viability of 4T1 cells treated with FA-ZA/IR780@HPNs at pH 6.5 was remarkably lower than that of cells incubated with the counterparts at pH 7.4 (Fig. 6b). A similar result was also attained for ZA/IR780@HPNs (Fig. S13d†). Moreover, the fluorescence staining of live/dead cells (Fig. 6c) revealed that 4T1 cells treated with FA-ZA/IR780@HPNs (ZA concentration = $3.13\ \mu\text{M}$; IR780 concentration = $0.38\ \mu\text{M}$) at pH 6.5 without laser irradiation showed remarkable PI-positive staining relative to cells treated with the counterparts at pH 7.4. It is worth noting that, at the same drug concentration without laser irradiation, the FA-ZA/IR780@HPNs at pH 6.5 exhibited higher cytotoxicity against 4T1 cells than ZA/IR780@HPNs at the same pH (Fig. 6b and S13d†). These findings strongly demonstrate that the dePEGylation and FA targeting of FA-ZA/IR780@HPNs in the weakly acidic milieu could effectively enhance their cellular internalization *via* FA receptor-mediated endocytosis, thus remarkably increasing the intracellular ZA concentration to induce cytotoxicity.

Notably, at low drug concentrations (ZA concentration = $6.25\ \mu\text{M}$ and IR780 concentration = $0.75\ \mu\text{M}$) with 5 min NIR laser irradiation, the viability of 4T1 cells treated with FA-ZA/

IR780@HPNs or ZA/IR780@HPNs at pH 6.5 was largely reduced compared to cells treated at pH 7.4 (Fig. 6d). Also, compared to ZA/IR780 mixtures, the FA-ZA/IR780@HPNs and ZA/IR780@HPNs significantly enhanced the anticancer activity of photothermal chemotherapy. These results signify that the developed FA-ZA/IR780@HPNs could show potent anticancer activity even at a low drug dosage against 4T1 cells owing to the promoted cellular internalization *via* acidity-activated PEG detachment and FA receptor-mediated endocytosis, NIR-induced IR780-mediated PTT combined with ZA chemotherapy. Surprisingly, it was found that, without NIR laser irradiation, the IR780@HPNs (IR780 concentration = 0.75 μM) showed the significant cytotoxicity toward 4T1 cells. This could be ascribed to that the mitochondrion targeting of IR780 molecules may cause cell apoptosis. Similar results were also attained in several nanoparticle-based IR780 delivery systems.^{47,48} Furthermore, with NIR laser irradiation, the IR780@HPNs exhibited more potent anticancer efficacy compared to ZA/IR780@HPNs (Fig. 6d). In view of the NIR-triggered singlet oxygen generation of IR780 molecules for cancer photodynamic therapy,^{49,50} it was assumed that the ionic pairings of positively-charged IR780 molecules with negatively-charged ZA molecules promoted the encapsulation of some IR780 molecules into the PLGA-rich core, thus hindering the diffusion of singlet oxygen to decline the NIR-elicited anticancer potency of ZA/IR780@HPNs.

3.7. *In vivo* biodistribution and NIR-triggered tumor hyperthermia

After the promoted uptake of FA-ZA/IR780@HPNs by 4T1 cells in a weakly acidic milieu mimicking the tumor extracellular environment was confirmed, the *in vivo* tumor accumulation of FA-ZA/IR780@HPNs and their biodistribution were studied using the subcutaneous 4T1 tumor model in female BALB/c mice. For comparison, the ZA/IR780@HPNs without FA ligands were adopted in this work. 4T1 tumor-bearing mice intravenously injected with various ZA/IR780-containing formulations were observed by *in vivo* IR780 fluorescence imaging. Obviously, at 24 and 48 h post-injection, compared to the ZA/IR780 mixture-treated group, the IR780-carrying HPN groups displayed stronger fluorescence signals in tumor regions (Fig. 7a and b). Such an appreciably increased deposition of IR780-loaded HPNs within tumor tissue could be ascribed to the EPR effect. Furthermore, in comparison with the ZA/IR780@HPN group, the FA-ZA/IR780@HPN group showed somewhat higher IR780 fluorescence intensities at the tumor sites over the time course. Also, compared to the tumor receiving the ZA/IR780 mixture possessing quite low *ex vivo* NIR fluorescence signals, the tumors treated with ZA/IR780-carrying HPNs showed remarkably higher NIR fluorescence signals, in particular for tumors treated with FA-ZA/IR780@HPNs (Fig. 7c and d). These results evidently demonstrate that the FA-ZA/IR780@HPNs could effectively deposit at the 4T1 tumor site upon FA-mediated tumor targeting activated by acidity-triggered dePEGylation. In contrast, due to the lack of FA targeting, the ZA/IR780@HPNs only showed moder-

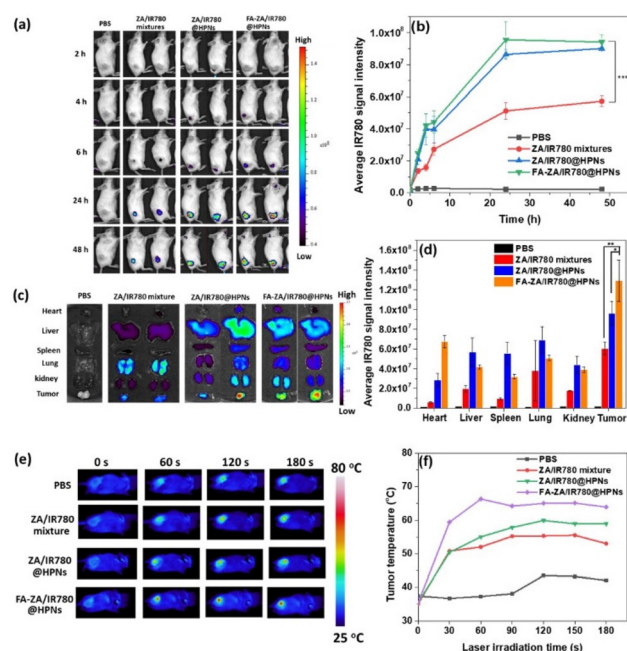


Fig. 7 (a) *In vivo* NIR images and (b) average IR780 fluorescence intensities of 4T1 tumor-bearing mice receiving intravenous injection of ZA/IR780 mixtures, ZA/IR780@HPNs and FA-ZA/IR780@HPNs, respectively, obtained by IVIS ($n = 3$). (c) Fluorescence images and (d) average IR780 fluorescence intensity of the isolated major organs and tumors from 4T1 tumor-bearing mice at 48 h post-injection of various formulations ($n = 3$). (e) Infrared thermographic images and (f) tumor temperature profiles of 4T1 tumor-bearing mice receiving various formulations and exposed to 3 min irradiation of an 808 nm NIR laser (1.25 W cm^{-2}) at 24 h post-injection.

ate tumor accumulation. On the other hand, as presented in the *ex vivo* NIR fluorescence images, compared to ZA/IR780 mixtures, the FA-ZA/IR780@HPNs and ZA/IR780@HPNs showed appreciable accumulation in the liver and spleen due to the inevitable uptake of nanoassemblies by the RES. Similar biodistributions of drug-carrying nanoparticles in tumor-bearing mice have been observed in other studies.^{51,52}

Under 808 nm laser irradiation (1.25 W cm^{-2}) for 3 min at 24 h post-injection of various formulations, in comparison with a slightly elevated temperature in the tumor of mice receiving PBS as an important control (Fig. 7e and f), the local tumor temperature of mice treated with IR780-containing HPNs or the ZA/IR780 mixture appreciably increased, revealing the effective NIR-triggered IR780-mediated hyperthermia on tumor. Notably, as compared to ZA/IR780 mixtures and ZA/IR780@HPNs, the FA-ZA/IR780@HPNs provoked significantly powerful NIR-activated hyperthermia on tumor (local temperature beyond $65 \text{ }^\circ\text{C}$) as a result of their massive accumulation in tumor tissue as presented in Fig. 7a and b.

3.8. *In vivo* tumor growth inhibition by photothermal chemotherapy

The *in vivo* antitumor abilities of various formulations in terms of the change in the relative tumor volume of 4T1

tumor-bearing mice were evaluated for up to 20 days post-treatment. As shown in Fig. 8a, 20 days after treatment and without laser irradiation, the relative tumor volume (V/V_0) of mice treated with ZA/IR780 mixtures was significantly increased by *ca.* 15-fold, being somewhat higher than that (*ca.* 10-fold) of mice treated with FA-ZA/IR780@HPNs. Apparently, the tumor-targeted single ZA-mediated chemotherapy delivered by FA-ZA/IR780@HPNs *via* the EPR effect displayed a limited suppression on tumor growth, while ZA/IR780 mixtures failed in inhibiting tumor growth due to their poor tumor accumulation. Note that, with laser irradiation, the tumor growth of mice treated with ZA/IR780@HPNs or FA-ZA/IR780@HPNs was appreciably impeded relative to that of mice receiving ZA/IR780 mixtures. This was also observed in the photographs of 4T1 tumor-bearing mice receiving different treatments for 20 days as shown in Fig. S14.† Similar results were also obtained in another tumor model, TRAMP-C1 prostate cancer cells (Fig. S15a†). The administration of ZA/IR780@HPNs or ZA/IR780 mixtures combined with NIR laser irradiation showed considerably delayed TRAMP-C1 tumor growth relative to its counterpart without irradiation. Moreover, TRAMP-C1 tumors harvested from the sacrificed mice treated with ZA/IR780@HPNs plus NIR irradiation were the smallest among the tumors receiving other treatments (Fig. S15b†). The

average TI (*ca.* 56.3%) of the combinatorial therapy provided by ZA/IR780@HPNs with NIR activation was markedly higher than that without NIR irradiation (39.3%) and that of ZA/IR780 mixtures with NIR illumination (42.8%) (Fig. S15c†). These findings clearly indicate that the ZA-mediated chemotherapy integrated with IR780-based PTT shows the antitumor effect superior to single ZA chemotherapy, and the tumor-targeted co-delivery of ZA and IR780 molecules *via* HPNs could remarkably boost the antitumor potency of photothermal chemotherapy.

More importantly, with laser irradiation, 4T1 tumor-bearing mice treated with FA-ZA/IR780@HPNs showed the significantly lower relative tumor volume compared to mice receiving ZA/IR780@HPNs (Fig. 8a). In agreement with the results of the *in vivo* tumor growth inhibition, most of the tumors isolated from the sacrificed mice treated with FA-ZA/IR780@HPNs plus laser irradiation almost completely disappeared in comparison with the tumors receiving other treatments (Fig. 8b). Furthermore, as presented in Fig. 8c, the average TI (*ca.* 84.9%) of FA-ZA/IR780@HPNs with NIR irradiation was remarkably higher than that of the counterparts without NIR irradiation (34.6%) and that of ZA/IR780@HPNs with NIR irradiation (62.4%). Based on the results of the *in vivo* biodistribution and antitumor studies, it can be concluded that the

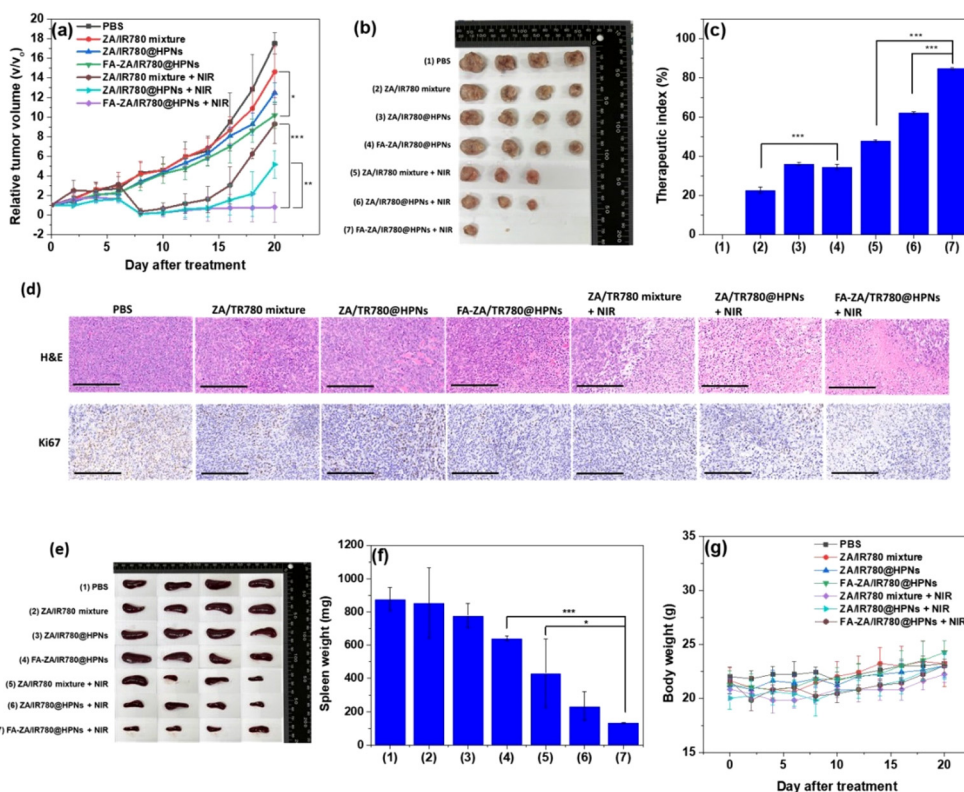


Fig. 8 (a) Tumor growth inhibition profiles of 4T1 tumor-bearing mice receiving various formulations with and without 808 nm NIR irradiation ($n = 4$). (b) Morphology and size of the tumors isolated from the euthanized mice at day 20 post-treatment. (c) TI value of different treatments ($n = 4$). (d) H&E and Ki67 staining images of tumor sections from 4T1 tumor-bearing mice receiving various treatments. Scale bars are 200 μm . (e) Morphology and (f) weight of the spleens collected from the euthanized mice at day 20 after the treatment ($n = 4$). (g) Body weight of 4T1 tumor-bearing mice receiving various treatments with and without 808 nm NIR irradiation ($n = 4$).

sufficient accumulation of FA-ZA/IR780@HPNs in 4T1 tumor sites by means of the tumor-activated FA-mediated targeting prominently augmented the antitumor potency of photothermal chemotherapy (Scheme 1). By contrast, in the absence of FA-mediated tumor targeting, the dual-modality therapy by ZA/IR780@HPNs was not able to inhibit tumor growth in an effective manner. On the other hand, the H&E staining images of the tumor sections (Fig. 8d) illustrated that most of the cancer cells within 4T1 tumor receiving PBS maintained their normal morphology, while the tumor cells treated with single ZA-mediated chemotherapy groups were slightly damaged. Notably, the tumors treated by photothermal chemotherapy with FA-ZA/IR780@HPNs showed more remarkable cell apoptosis and necrosis as compared to those receiving the combined therapy using either ZA/IR780@HPNs or ZA/IR780 mixtures. Also, for the tumor sections from the FA-ZA/IR780@HPN group with NIR laser irradiation, a significant reduction in the expression level of Ki67 was observed relative to other groups. Undoubtedly, the FA-ZA/IR780@HPNs display powerful anti-proliferative effects on xenograft tumors by tumor-targeted photothermal chemotherapy.

In the late stages of aggressive breast cancer, splenomegaly caused by the leukemoid reactions is known to be a vital clinical symptom.^{53,54} As presented in Fig. 8e and f, the volume and weight of the spleens harvested from 4T1 tumor-bearing mice treated with FA-ZA/IR780@HPNs combined with NIR irradiation were the smallest among those of mice receiving other treatments. Besides, no significant metastasis of cancer cells was observed in the major organs of 4T1 tumor-bearing mice treated with FA-ZA/IR780@HPNs or ZA/IR780@HPNs with NIR irradiation (Fig. S16[†]), whereas the appreciable metastasis of cancer cells into important organs was found in other treatment groups.

These data further demonstrate that the FA-ZA/IR780@HPNs not only effectively kill 4T1 cells by photothermal chemotherapy but also suppress migration of 4T1 cells by the ZA-mediated effect, thereby largely inhibiting 4T1 tumor growth and cancer cell invasion into major organs. It should be mentioned that these formulations used in this study did not lead to serious acute toxicity because no obvious variation in the body weight of the treated mice over time in all groups was observed (Fig. 8g).

4. Conclusions

To maximize the antitumor efficacy of the photothermal chemotherapy, the FA-ZA/IR780@HPNs capable of achieving tumor-activated targeting by detaching PEG shielding were developed in this work. The FA-ZA/IR780@HPNs exhibited satisfactory drug loading capacity and robust colloidal stability in a serum-containing milieu. Also, the FA-ZA/IR780@HPNs not only enhanced the photostability and photothermal conversion efficiency of IR780 molecules, but also prevented premature drug leakage. The *in vitro* cellular uptake and cytotoxicity studies showed the FA exposure of FA-ZA/IR780@HPNs in a

mimic acidic tumor microenvironment because PEG detachment significantly promoted their internalization by 4T1 cancer cells, thus giving rise to a potent anticancer activity based on photothermal chemotherapy. Also, the FA-ZA/IR780@HPNs remarkably suppressed the migration of 4T1 cells. Importantly, after being efficiently deposited within 4T1 tumors, the FA-ZA/IR780@HPNs induced strong hyperthermia on tumors under NIR laser irradiation. By the IR780-mediated photothermal therapy combined with ZA chemotherapy, the FA-ZA/IR780@HPNs prominently suppressed tumor growth *in vivo* and metastasis. Based on these findings, the designed FA-ZA/IR780@HPNs could realize sufficient tumor accumulation, cellular internalization and photothermal chemotherapy, thereby displaying their great potential in boosting the therapeutic efficacy for aggressive breast cancer.

Conflicts of interest

There are no conflicts to declare.

Acknowledgements

This work is supported by the National Science and Technology Council (MOST 110-2628-E-005-001, MOST111-2628-E-005-009-MY2), National Chung Hsing University and Chung Shan Medical University (NCHU-CSMU 11202), Taiwan.

References

- 1 C. C. Hung, W. C. Huang, Y. W. Lin, T. W. Yu, H. H. Chen, S. C. Lin, W. H. Chiang and H. C. Chiu, *Theranostics*, 2016, **6**, 302–317.
- 2 W. Ni, J. Wu, H. Fang, Y. Feng, Y. Hu, L. Lin, J. Chen, F. Chen and H. Tian, *Nano Lett.*, 2021, **21**, 7796–7805.
- 3 J. Nam, S. Son, L. J. Ochyl, R. Kuai, A. Schwendeman and J. J. Moon, *Nat. Commun.*, 2018, **9**, 1074.
- 4 Y. Zou, D. Huang, S. He, X. Song, W. Liu, W. Sun, J. Du, J. Fan and X. Peng, *Chem. Sci.*, 2023, **14**, 1010–1017.
- 5 H. J. Yoon, H. S. Lee, J. H. Jung, H. K. Kim and J. H. Park, *ACS Appl. Mater. Interfaces*, 2018, **10**, 6118–6123.
- 6 Z. Cai, Y. Zhang, Z. He, L. P. Jiang and J. J. Zhu, *ACS Appl. Bio Mater.*, 2020, **3**, 5322–5330.
- 7 X. Zhu, L. Li, J. Tang, C. Yang, H. Yu, K. Liu, Z. Zheng, X. Gu, Q. Yu, F. J. Xu and Z. Gan, *Biomaterials*, 2022, **280**, 121305.
- 8 M. H. Hsieh, T. H. Wang, S. H. Hu, T. C. Hsu, J. L. Yow, B. S. Tzang and W. H. Chiang, *Chem. Eng. J.*, 2022, **446**, 137243.
- 9 L. Yang, X. Hou, Y. Zhang, D. Wang, J. Liu, F. Huang and J. Liu, *J. Controlled Release*, 2021, **339**, 114–129.
- 10 H. Liu, C. Xu, M. Meng, S. Li, S. Sheng, S. Zhang, W. Ni, H. Tian and Q. Wang, *Acta Biomater.*, 2022, **144**, 132–141.
- 11 W. Jiang, H. Zhang, J. Wu, G. Zhai, Z. Li, Y. Luan and S. Garg, *ACS Appl. Mater. Interfaces*, 2018, **10**, 34513–34523.

- 12 H. Y. Yang, M. S. Jang, G. H. Gao, J. H. Lee and D. S. Lee, *Polym. Chem.*, 2016, **7**, 1813–1825.
- 13 J. M. Harris and R. B. Chess, *Nat. Rev. Drug Discovery*, 2003, **2**, 214–221.
- 14 F. M. Veronese and G. Pasut, *Drug Discovery Today*, 2005, **10**, 1451–1458.
- 15 Y. Fang, J. Xue, S. Gao, A. Lu, D. Yang, H. Jiang, Y. He and K. Shi, *Drug Delivery*, 2017, **24**, 22–32.
- 16 L. Kong, F. Campbell and A. Kros, *Nanoscale Horiz.*, 2019, **4**, 378–387.
- 17 N. Guo, Y. Zhou, T. Wang, M. Lin, J. Chen, Z. Zhang, X. Zhong, Y. Lu, Q. Yang, D. Xu, J. Gao and M. Han, *ACS Appl. Mater. Interfaces*, 2020, **12**, 57798–57809.
- 18 Z. Yang, N. Sun, R. Cheng, C. Zhao, Z. Liu, X. Li, J. Liu and Z. Tian, *Biomaterials*, 2017, **147**, 53–67.
- 19 X. Zeng, G. Liu, W. Tao, Y. Ma, X. Zhang, F. He, J. Pan, L. Mei and G. Pan, *Adv. Funct. Mater.*, 2017, **27**, 1605985.
- 20 Y. N. Hung, Y. L. Liu, Y. H. Chou, S. H. Hu, B. Cheng and W. H. Chiang, *Eur. Polym. J.*, 2022, **163**, 110944.
- 21 L. Zhu, P. Kate and V. P. Torchilin, *ACS Nano*, 2012, **6**, 3491–3498.
- 22 Z. Zou, X. He, D. He, K. Wang, Z. Qing, X. Yang, L. Wen, J. Xiong, L. Li and L. Cai, *Biomaterials*, 2015, **58**, 35–45.
- 23 S. Y. Huang, N. T. Yeh, T. H. Wang, T. C. Hsu, H. Y. Chin, B. S. Tzang and W. H. Chiang, *Int. J. Biol. Macromol.*, 2023, **227**, 925–937.
- 24 T. Liao, C. Liu, J. Ren, H. Chen, Y. Kuang, B. Jiang, J. Chen, Z. Sun and C. Li, *Int. J. Biol. Macromol.*, 2021, **183**, 2017–2029.
- 25 W. C. Huang, S. H. Chen, W. H. Chiang, C. W. Huang, C. L. Lo, C. S. Chern and H. C. Chiu, *Biomacromolecules*, 2016, **17**, 3883–3892.
- 26 L. Zhong, L. Xu, Y. Liu, Q. Li, D. Zhao, Z. Li, H. Zhang, H. Zhang, Q. Kan, Y. Wang, J. Sun and Z. He, *Acta Pharm. Sin. B*, 2019, **9**, 397–409.
- 27 Y. Li, J. Lin, P. Wang, Q. Luo, F. Zhu, Y. Zhang, Z. Hou, X. Liu and J. Liu, *Nano-Micro Lett.*, 2020, **12**, 182.
- 28 Y. Zhao, B. Han, J. Hao, Y. Zheng, J. Chai, Z. Zhang, Y. Liu and L. Shi, *Nano Today*, 2021, **41**, 101313.
- 29 Y. H. Chou, Y. L. Liu, T. C. Hsu, J. L. Yow, B. S. Tzang and W. H. Chiang, *J. Mater. Chem. B*, 2022, **10**, 4363–4374.
- 30 W. Lei, C. Sun, T. Jiang, Y. Gao, Y. Yang, Q. Zhao and S. Wang, *Mater. Sci. Eng., C*, 2019, **105**, 110103.
- 31 Y. Lia, W. Hong, H. Zhang, T. T. Zhang, Z. Chen, S. Yuan, P. Peng, M. Xiao and L. Xu, *J. Controlled Release*, 2020, **317**, 232–245.
- 32 M. C. Xiao, Y. H. Chou, Y. N. Hung, S. H. Hu and W. H. Chiang, *Mater. Sci. Eng., C*, 2020, **116**, 111277.
- 33 Y. Kuang, K. Zhang, Y. Cao, X. Chen, K. Wang, M. Liu and R. Pei, *ACS Appl. Mater. Interfaces*, 2017, **9**, 12217–12226.
- 34 C. Jiang, H. Cheng, A. Yuan, X. Tang, J. Wu and Y. Hu, *Acta Biomater.*, 2015, **14**, 61–69.
- 35 S. K. Rajendrakumar, N. C. Chang, A. Mohapatra, S. Uthaman, B. I. Lee, W. B. Tsai and I. K. Park, *Int. J. Mol. Sci.*, 2018, **19**, 1189.
- 36 S. Y. Lin, R. Y. Huang, W. C. Liao, C. C. Chuang and C. W. Chang, *Nanotheranostics*, 2018, **2**, 106–116.
- 37 H. Xu, D. Yang, C. Cai, J. Gou, Y. Zhang, L. Wang, H. Zhong and X. Tang, *Acta Biomater.*, 2015, **16**, 156–168.
- 38 H. H. Chen, I. L. Lu, T. I. Liu, Y. C. Tsai, W. H. Chiang, S. C. Lin and H. C. Chiu, *Colloids Surf., B*, 2019, **177**, 294–305.
- 39 H. K. Makadia and S. J. Siegel, *Polymers*, 2011, **3**, 1377–1397.
- 40 W. Ou, L. Jiang, R. K. Thapa, Z. C. Soe, K. Poudel, J. H. Chang, S. K. Ku, H. G. Choi, C. S. Yong and J. O. Kim, *Theranostics*, 2018, **8**, 4574–4590.
- 41 Y. J. Lu, T. S. Anilkumar, C. C. Chuang and J. P. Chen, *Cancers*, 2021, **13**, 3690.
- 42 F. Benyettou, M. Alhashimi, M. O'Connor, R. Pasricha, J. Brandel, H. Traboulsi, J. Mazher, J. C. Olsen and A. Trabolsi, *ACS Appl. Mater. Interfaces*, 2017, **9**, 40006–40016.
- 43 J. A. Joyce and J. W. Pollard, *Nat. Rev. Cancer*, 2009, **9**, 239–252.
- 44 H. Geng, M. Zhou, B. Li, L. Liu, X. Yang, Y. Wen, H. Yu, H. Wang, J. Chen and L. Chen, *Chem. Eng. J.*, 2021, **417**, 128103.
- 45 J. Mani, S. Vallo, K. Barth, J. Makarević, E. Juengel, G. Bartsch and C. Wiesner, *Prostate Cancer Prostatic Dis.*, 2012, **15**, 250–255.
- 46 H. Liu, S. H. Wang, S. C. Chen, C. Y. Chen and T. M. Lin, *BMC Cancer*, 2019, **19**, 176.
- 47 G. Capistrano, A. A. Sousa-Junior, R. A. Silva, F. Mello-Andrade, E. R. Cintra, S. Santos, A. D. Nunes, R. M. Lima, N. Zufelato, A. S. Oliveira, M. Pereira, C. H. Castro, E. M. Lima, C. G. Cardoso, E. Silveira-Lacerda, S. A. Mendanha and A. F. Bakuzis, *ACS Biomater. Sci. Eng.*, 2020, **6**, 4523–4538.
- 48 Y. Wang, T. Liu, E. Zhang, S. Luo, X. Tan and C. Shi, *Biomaterials*, 2014, **35**, 4116–4124.
- 49 G. Yang, J. Tian, C. Chen, D. Jiang, Y. Xue, C. Wang, Y. Gao and W. Zhang, *Chem. Sci.*, 2019, **10**, 5766–5772.
- 50 Z. Mo, M. Qiu, K. Zhao, H. Hu, Q. Xu, J. Cao, Y. Luo, L. Liu, Z. Xu, C. Yi, Z. Xiong, G. Liao and S. Yang, *J. Colloid Interface Sci.*, 2022, **611**, 193–204.
- 51 X. Zhang, R. Zhang, J. Huang, M. Luo, X. Chen, Y. Kang and J. Wu, *J. Mater. Chem. B*, 2019, **7**, 3537–3545.
- 52 M. Y. Shen, T. I. Liu, T. W. Yu, R. Kv, W. H. Chiang, Y. C. Tsai, H. H. Chen, S. C. Lin and H. C. Chiu, *Biomaterials*, 2019, **197**, 86–100.
- 53 N. Xu, A. Hu, X. Pu, J. Li, X. Wang, J. Wang, Z. Huang, X. Liao and G. Yin, *ACS Appl. Mater. Interfaces*, 2022, **14**, 15894–15910.
- 54 M. Liu, X. Jin, X. He, L. Pan, X. Zhang and Y. Zhao, *PLoS One*, 2015, **10**, e0121921.